Proceedings of the 21st ICSMGE, Vienna, Austria, 14 – 19 June 2026. Pistrol, Adam & Schweiger (eds.)
Published by: ÖGG, Austrian Society for Geomechanics, Salzburg, Austria, ISBN 978-3-9503898-4-5
https://doi.org/10.53243/ICSMGE2026-2304

Development of an expansive bedrock model considering differences in exchangeable cation species between clay mineral crystalline layers

Keitaro Hoshi, Shotaro Yamada, Yuta Abe
Graduate School of Engineering, Department of Civil Engineering, Tohoku University, Sendai, Japan,
keitaro.hoshi.r2@dc.tohoku.ac.jp

ABSTRACT: Bedrocks containing expansive clay minerals cause many problems in tunnel construction and post-construction maintenance. In addition to the elastoplastic behavior of geomaterials, electro-chemical interactions between clay mineral crystalline layers and interlayer ionic species have a significant influence on mechanical behavior of swelling. Therefore, it is necessary to understand the swelling phenomena by paying attention to microscopic information such as exchangeable cation species. No multiphysics constitutive model has been proposed that clearly distinguishes the different swelling behavior depending on the exchangeable cation species and couples the elastoplastic behavior of bedrock with the electro-chemical phenomena occurring between crystalline layers. This study proposes an expansive bedrock model capable of describing different swelling behaviors caused by exchangeable cation species. We previously proposed a numerically robust multiphysics elastoplastic model of expansive bedrock that can be applied to large deformation problems by proposing a new decomposition method for the deformation gradient. Thus, this study introduced a double-layer repulsive force based on the Stern theory to our previously proposed model. We performed tunnel excavation and swelling analysis using a finite element analysis code, incorporating the proposed model. Results varied depending on the exchangeable cation species in the interlaminar region; for sodium-type smectite, significant swelling only occurred in the tunnel bottom; this did not occur for calcium- and potassium-type smectite. We elucidated the basic mechanism of tunnel road deformation, including different swelling behaviors due to different exchangeable cation species, highlighting the multiscale and multiphysics interactions of electrochemical phenomena in interlaminar regions and elastoplastic phenomena in bedrock.

KEYWORDS: Expansive bedrock, tunnel, finite deformation, Stern theory, multiphysics.

1 INTRODUCTION

Bedrocks containing expansive clay minerals cause many problems in tunnel construction and post-construction maintenance. In addition to the elastoplastic behavior of geomaterials, electro-chemical interactions between clay mineral crystalline layers and interlayer ionic species significantly influence the mechanical behavior of swelling. Thus, swelling is a complex multiphysics phenomenon that is difficult to predict quantitatively.

We developed a constitutive model of expansive bedrock (Hoshi et al., 2022; 2024) by integrating an elastoplastic model that considers electro-chemical-mechanical interactions between crystal layers (Kyokawa et al., 2020) and a Cam-clay model that considers cementation and its degradation (Yamada et al., 2022). However, the conventional expansive bedrock model, including our model, could not describe the different swelling behavior depending on the exchangeable cation species existing between crystalline layers. Therefore, they could not represent the differences in tunneling deformation caused by the major cation species present in smectite. In this study, we propose a novel multiphysics model that can describe differences due to cation species by introducing the electric double-layer repulsive force considering the Stern layer proposed by Hoshi et al., (2025) into our constitutive model (Hoshi et al., 2024). Moreover, we clarify the effect of interlayer ions on the tunneling deformation by demonstrate tunnel excavation and swelling analysis.

2 FINITE DEFORMATION EXPANSIVE BEDROCK MODEL

Hoshi et al. (2024) proposed a robust finite deformation model that couples the elastoplastic behavior of a bedrock with the electro-chemical phenomena occurring between crystal layers. Our proposed model assumes a double porous structure consisting of bedrock skeleton voids and interlaminar voids. The differential volume in the reference configuration dV is additively decomposed into an interlaminar void volume dV^{il}, which involves expansive clay minerals, and a differential bedrock skeleton volume dV^{ss}, which includes other pores.

$$\boldsymbol{dV = dV^{ss} + dV^{il}} \tag{1}$$

The differential volume of each skeleton is defined as

$$\boldsymbol{dV^{ss} = \theta_0^{ss} dV}, \quad \boldsymbol{dV^{il} = \theta_0^{il} dV}, \tag{2}$$

where θ_0^{ss} and θ_0^{il} denote the initial volume fractions of each skeleton. These are defined as follows to satisfy $\theta_0^{\mathrm{ss}} + \theta_0^{\mathrm{il}} = 1$:

$$\boldsymbol{\theta_0^{ss} = \frac{1 + e_0^{ss}}{1 + e_0}}, \quad \boldsymbol{\theta_0^{il} = \frac{1 + e_0^{il}}{1 + e_0}}, \tag{3}$$

where e_0 denotes the total initial void ratio, e_0^{il} denotes the interlaminar initial void ratio, and e_0^{ss} denotes the initial void ratio of the bedrock skeleton.

Based on the double porous structure, the deformation gradients from the two skeletons are defined, as shown in Figure 1. These include the deformation of the bedrock skeleton $\boldsymbol{F}^{\mathrm{ss}}$ from its differential volume dV^{ss} and the deformation of the interlaminar skeleton $\boldsymbol{F}^{\mathrm{il}}$ from its differential volume dV^{il}. The proposed model assumes that the deformation $\boldsymbol{F}^{\mathrm{ss}}$ is similar to the total deformation $\boldsymbol{F}$ of expansive bedrock. For simplicity, the deformation $\boldsymbol{F}^{\mathrm{il}}$ of the interlaminar skeleton is assumed to be an isotropic expansion or contraction deformation from a macroscopic perspective.

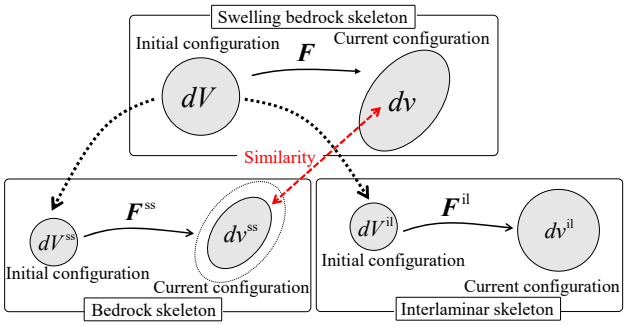

Figure 1. Decomposition of deformation.

Based on the above assumptions, the deformation of each skeleton is determined so that the volume change J of the expansive rock satisfies the following relationship with the volume changes $J^{ss}(=\det \boldsymbol{F}^{ss})$ and $J^{il}(=\det \boldsymbol{F}^{il})$ of each skeleton.

$$\boldsymbol{J = J^{ss}\theta_0^{ss} + J^{il}\theta_0^{il}} \tag{4}$$

The deformation of the bedrock skeleton $\boldsymbol{F}^{ss}$ is defined as follows with isotropic deformation component $\widehat{\boldsymbol{F}}$:

$$\boldsymbol{F^{ss} = (J^{ss})^{1/3}\widehat{F}}. \tag{5}$$

Therefore, following relationship holds for $\boldsymbol{F}$ and $\boldsymbol{F}^{ss}$.

$$\boldsymbol{F^{ss} = \left(\frac{J^{ss}}{J}\right)^{1/3} F}. \tag{6}$$

The deformation of the bedrock skeleton, $\boldsymbol{F}^{ss}$, is determined according to the framework of finite deformation elastoplastic theory based on the multiplicative decomposition of the deformation gradient. $\boldsymbol{F}^{ss}$ is multiplicatively decomposed into the elastic $\boldsymbol{F}^{e}$ and plastic $\boldsymbol{F}^{p}$ components

$$\boldsymbol{F^{ss} = F^{e}F^{p}}. \tag{7}$$

In this study, the finite-deformation Cam-clay model proposed by Abe et al. (2024), with a method to consider cementation and its degradation proposed by Yamada et al. (2022), was used as an elastoplastic model. The proposed model translates the yield surface in the Cauchy stress space to the tensile side, as shown in Figure 2. As a result, the proposed model describes the tensile strength arising from the cementation effect of bedrock skeleton materials, such as cement-treated soil and bedrock. Moreover, the model describes the internal structural degradation of bedrock by eliminating the parallel shift in the figure due to plastic deformation.

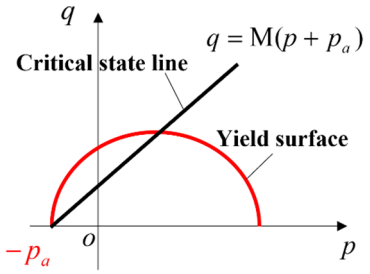

Figure 2. Parallel shift of yield surface.

The deformation of interlaminar skeleton $\boldsymbol{F}^{il}$ is assumed to consist only of a volume change component and the volume change J^{il} is as follows:

$$\boldsymbol{F^{il} = \left(J^{il}\right)^{1/3} I},\ \boldsymbol{J^{il} = \frac{d}{d_0}} \tag{8}$$

where d_0 and d are the initial and current interlaminar distances, respectively.

The interlaminar distance is determined by the following equilibrium equation for the electrochemical–mechanical forces between the crystal layers:

$$\boldsymbol{f_a(d) - f_r(c,d) - f_h(d) + f_e(\sigma) = 0} \tag{9}$$

where c is the ion concentration of the pore fluid, f_a is the Van der Waals force, f_r is the osmotic pressure from the double diffusion layers, f_h is the hydration force, and f_e is the force from the mean effective stress. The osmotic pressure, van del Waals force, and hydration force are monotonically decreasing functions with respect to the interlaminar distance; moreover, the osmotic pressure changes with ion concentration.

3 DOUBLE LAYER FORCE CONSIDERING THE STERN LAYER

In this study, we introduce the double-layer repulsive force (Hoshi et al., 2025) considering the Stern model, which is an improved model of the Gouy-Chapman diffusion layer model, into the model presented in Section 2. The following equation, derived by Verwey and Overbeek (1948), is used as the charge in the Stern layer to account for the cation species and finite size of ions:

$$\boldsymbol{\Omega_1 = \frac{N_1 ze}{1 + \frac{\rho_w}{Mc} exp\left[-\left(\frac{ze\psi_\delta + \phi}{kT}\right)\right]}}, \tag{10}$$

where z is the ion valence, e is the electronic charge, ρ_w is the density of solvent, M is the molar mass of the solvent, ψ_δ is the zeta potential, k is the Boltzmann's constant, T is the absolute temperature. By applying Equation (10), the proposed model can consider two specific properties of exchangeable cations: N_1, ϕ. N_1 is the number of adsorption spots for counter ions per unit square and varies according to hydration radius. ϕ represents the specific adsorption potential, which is a unique adsorption property of ions. In this study, the clay mineral surfaces were assumed to have a constant charge. The electric charges of the clay mineral surface Ω and the Gouy layer Ω_2 are as follows:

$$\boldsymbol{\Omega_1 = 96.5 \times \left(\frac{EXC}{S}\right)}, \tag{11}$$

$$\boldsymbol{\Omega_2 = \sqrt{8cN_A\epsilon kT}\, sinh\left(\frac{ze\psi_\delta}{2kT}\right)}, \tag{12}$$

where EXC is the exchange capacity, S is the specific surface area, N_A is Avogadro's constant, ϵ is the static permittivity of pore fluid. If the ion concentration of the pore fluid is known, then the zeta potential ψ_δ is uniquely determined to satisfy the following electrical neutrality condition:

$$\boldsymbol{\Omega = \Omega_1 + \Omega_2}, \tag{13}$$

The interlayer center is assumed to exist in the Gouy layer. A nondimensional electric potential u_d is derived using ψ_δ which satisfies electric neutral condition as follows.

$$\boldsymbol{u_d = 8\, tanh^{-1}\left[exp\left(-\omega(d - \delta)\, tanh\left(\frac{ze\psi_\delta}{4kT}\right)\right)\right]}, \tag{14}$$

δ is the distance from the clay mineral surface to the Stern surface, and ω is the Debye–Hückel parameter as shown in following equation.

$$\boldsymbol{\omega = \sqrt{\frac{2cN_A z^2 e^2}{\epsilon kT}}} \tag{15}$$

Finally, repulsive force from the double diffusion layer considering the Stern layer f_r is derived as follows.

$$\boldsymbol{f_r = 2cN_A kT(cosh\, u_d - 1)} \tag{16}$$

In this study, we consider the electro-chemical-mechanical equilibrium between crystal layers as follows using Equation (16).

$$\boldsymbol{f^{il}(c,d,\sigma) = f_a - f_r - f_h + f_e = 0} \tag{17}$$

This equilibrium includes the van der Waals force f_a, hydration force f_h, and effective stress f_e. The effective stress

is calculated by coupling the elastoplastic constitutive law of the bedrock skeleton (the modified Cam–Clay model considering the cementation effect and its degradation).

4 NUMERICAL EXAMPLE

We performed the tunnel excavation and swelling analysis results obtained using an in-house finite element analysis code, including the proposed model. Figure 3 shows the finite element model (5040 nodes and 2400 elements). A tunnel was placed at the center of the analysis region (100 × 100 × 1 m), and calculations were performed assuming planar strain conditions. Horizontal displacements were fixed at the left and right boundaries, and vertical displacements were fixed at the lower boundary. A uniformly distributed load of 1000 kPa, equivalent to the earth pressure produced by an earth cover height of approximately 50 m, was applied to the top boundary to reproduce approximately 100 m of earth cover at the point where deformation occurred in the Mt. Sakazuki Tunnel in Japan. The analyzed parameters were set based on the report for the deformation at Mt. Sakazuki Tunnel (Okui et al. 2009).

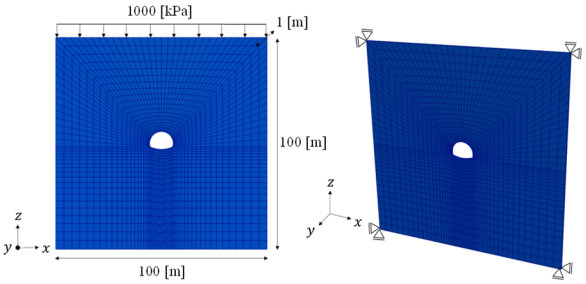

Figure 3. Finite element model and boundary conditions.

In this study, we analyzed three cases in which the bedrock contained sodium-, calcium-, or potassium-type expansive clay minerals. The swelling analysis was performed by uniformly decreasing the pore fluid ion concentration over the entire analysis area after the excavation analysis was completed. Although ion concentration changes are likely to occur nonuniformly owing to the heterogeneity of the groundwater flow, Hoshi et al. (2022) demonstrated that even under simplified conditions, the fundamental mechanism of tunnel load failure can be meaningfully analyzed. Figure 4 shows the cementation distribution after the swelling analysis. Here, the cementation value corresponds to translation magnitude of the yield surface in Figure 2.

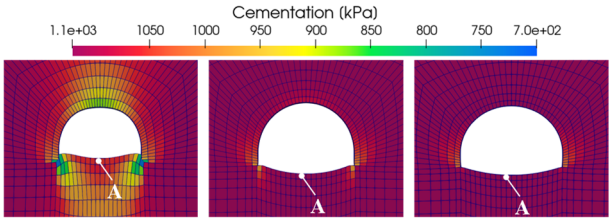

(a) Na^+ (b) Ca^{2+} (c) K^+

Figure 4. Cementation distribution after swelling analysis.

In the swelling analysis following the excavation with sodium-type smectite, cementation degradation and swelling progressed within a limited area, such as directly beneath the tunnel bottom, even though the ion concentration was uniformly reduced throughout the entire analysis area. Figure 5 shows the distributions of the vertical displacement and expansion in the bedrock immediately below the tunnel bottom in the case of sodium-type. The depth from the bottom was plotted on the vertical axis, and the cumulative values were plotted at a fixed point approximately 10 m from the bottom. The expansion and vertical displacement increased remarkably from approximately 5 m below the bottom. Due to space limitations, the figure is not included; however, this tendency matches the observed result for the Mt. Sakazuki Tunnel.

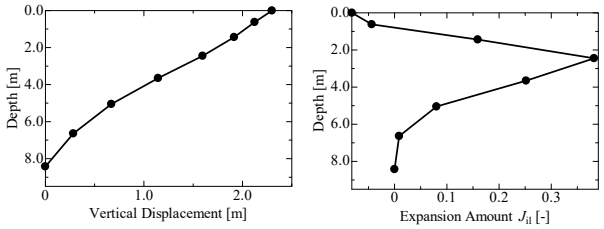

Figure 5. Distributions of deformations just below the tunnel bottom.

While large deformation was observed in the sodium-type, the internal degradation and tunnel road deformation were smaller for the calcium type. Consequently, the uplift of the tunnel roads did not occur. Moreover, swelling deformation was not observed in the case of the potassium-type smectite. These results indicate that the degree of tunnel road deformation varies significantly owing to the interlaminar exchangeable cation species present in the clay mineral interlayers. It is important to note that when the Gouy theory of electric double-layer repulsive force is applied, the difference between ionic species can only be evaluated in terms of valence, so that in the conventional model cannot be difference between sodium- and potassium-type with the same valence.

Next, we investigate the reasons for the differences in tunnel road deformation, as shown in Figure 4, from the perspective of the mechanical behavior beneath the tunnel base. Figure 4-6 show the stress path of the elements directly beneath the tunnel (Element A is shown in Figure 4) and the relationship between the ion concentration and the volumetric strain in each skeleton $\varepsilon_v^{ss}(=-\ln J^{ss})$, $\varepsilon_v^{il}(=-\ln J^{il})$ for each exchangeable ion species. The volumetric strains are positive under compression.

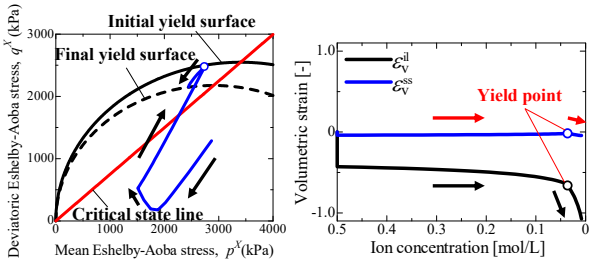

(a) (b)

Figure 6. Stress path and volumetric strain change (Na^+).

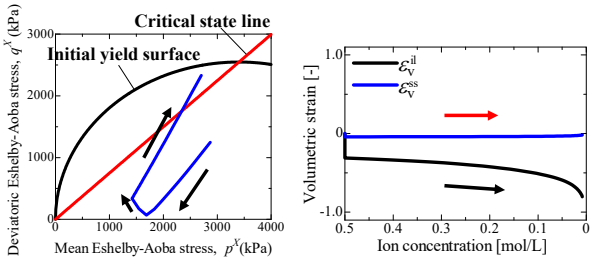

(a) (b)

Figure 7. Stress path and volumetric strain change (Ca^{2+}).

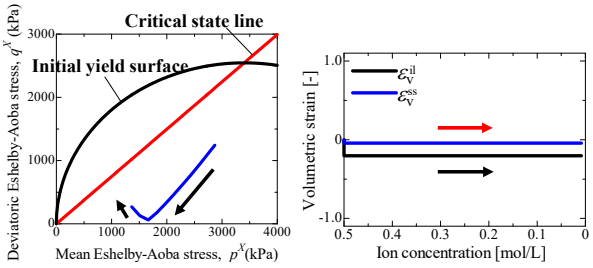

(a) (b)

Figure 8. Stress path and volumetric strain change (K^+).

In the swelling analysis following the excavation analysis with sodium-type smectite, an increase in the effective stress was observed owing to the influence of interlayer expansion with decreasing ion concentration, resulting in the yielding of element A above the critical state line, as shown in Figure 6(a). In the Cam-clay model, the area above the critical-state line is a softening zone with plastic expansion (Asaoka et al., 1994). This indicates that softening with plastic deformation occurs in the region with pronounced swelling because the mean effective stress and shear stress decrease after yielding. As the mean effective stress decreases owing to softening, the distance between the crystalline layers also increases, according to the mechanism described by Equation (17), leading to significant swelling directly below the tunnel base. Moreover, the rigidity of the bedrock decreases owing to the degradation of cementation as plastic deformation progresses. Consequently, swelling deformation increases because of the increased shear deformation and softening. In addition, comparing Figure 6 (a) and Figure 6 (b), it is evident that rapid swelling begins when the bedrock skeleton reaches a yield point. This result indicates that a decrease in ion concentration causes the yielding of the bedrock skeleton, which subsequently causes significant swelling in the interlaminar skeleton due to the softening of the bedrock skeleton. Therefore, the deterioration of tunnel roads is attributed to the multiscale interaction of microscopic electrochemical and macroscopic plastic-mechanical phenomena.

In the swelling analysis with calcium-type smectite, Figure 7(a) shows that the effective mean stress and shear stress also increase owing to the influence of interlayer expansion due to a decrease in ion concentration. However, the increase is smaller than that of the sodium type, and the bedrock skeleton does not yield. In addition, Figure 8(a) shows no increase in the effective stress due to a decrease in the ion concentration in the case of potassium-type smectite. Consequently, the bedrock skeleton did not reach the same yield as the calcium type. This is because of the reduction in the electric charge in the Gouy layer, which is caused by the smaller hydration radius of potassium than those of sodium and calcium ions, along with the specific adsorption phenomena on silica sheets of clay minerals; together, these factors cause a reduction in the double-layer repulsive force (Hoshi et al., 2025).

In summary, tunnel road deformation varies depending on whether the bedrock skeleton yields, with yielding being influenced by the exchangeable cation species in expansive clay minerals. Moreover, the computational results reveal that the significant swelling deformation beneath the tunnel bottom results from the interaction between microscopic interfacial chemical phenomena on the clay mineral surfaces and the macroscopic plastic mechanical phenomena in the bedrock skeleton.

5 CONCLUSION

This study proposes a novel numerical model for expansive bedrock by combining the methods of Hoshi et al. (2024) and Hoshi et al. (2025). Moreover, tunnel excavation and swelling analyses were conducted by applying the proposed model to the finite element method, assuming that the bedrock contained different exchangeable cation species. The simulation results revealed the difference in swelling behavior due to the exchangeable cation species. In addition, tunnel road deformation varied depending on whether the bedrock skeleton yielded, which in turn was influenced by the type of exchangeable cation species present in the expansive clay minerals. For sodium-type smectite, a significant increase in the effective stress was observed owing to the high swelling pressure, which attempted to expand the interlayers. This caused the softening, internal degradation, and yielding of the bedrock, leading to significant swelling of the interlaminar skeleton, which further accelerated the degradation of the bedrock skeleton. We elucidated that this negative spiral was the basic mechanism of the tunnel road uplift. However, for the calcium and potassium type smectite, the increase in effective stress was smaller owing to their lower swelling ability compared to that of the sodium type. As a result, the bedrock skeleton does not yield, and the destruction of tunnel roads owing to the multiscale and multiphysics interaction of the interlaminar skeleton and bedrock skeleton does not occur.

6 ACKNOWLEDGEMENTS

This study is supported by the Japan Tunneling Association, JST SPRING, and Grant-in-Aid for JSPS Fellows. (Grant Nos. JTA-R6-G1, JPMJSP2114, JP25KJ0576).

7 REFERENCES

Abe, Y., Yamada, S., Hoshi, K., Kyoya, T., 2024. Reconstruction of Cam-clay model based on multiplicative decomposition of the deformation gradient, *Comput. Geotech*. 166, 105958.

Asaoka, A., Nakano, M., Noda., 1994. Soil–water coupled behaviour of saturated clay near/at critical state, *Soils Found*. 34, 91–105.

Hoshi, K., Yamada, S., Kyoya, T., 2022. Finite Element Analysis of Expansive Bedrock Considering Electro-chemo-mechanical Coupling Phenomena in Crystal Layers of Clay Minerals and Internal Structural Degradation, *Rock Mech. Rock Eng*. 55, 7387-7407.

Hoshi, K., Yamada, S., Abe, Y., Kyoya, T., 2024. Construction of a multiphysics model for swelling bedrock based on a novel deformation gradient decomposition method, *Comput. Geotech*. 176, 106736.

Hoshi, K., Yamada, S., Kyoya, T., 2025. Multiphysics model of swelling geomaterials based on Stern theory: Describing different swelling behaviors depending on exchangeable cation species, *J. Rock Mech. Geotech. Eng*. (in press).

Kyokawa, H., Ohno, S., Kobayashi, I., 2020. A method for extending a general constitutive model to consider the electro-chemo-mechanical phenomena of mineral crystals in expansive soils, *Int. J. Numer. Anal. Meth. in Geomech*. 44, 749-771.

Okui, Y., Tsuruhara, T., Ota H, Sakuma, S., Nakata, C., 2009. Analysis of heaving behavior in Sakazukiyama road tunnel under use. *Proc. Tunnel Eng*., 19:, 173–180 (in Japanese)

Stern, O., 1924. Zur Theorie der Elektrolytischen Doppelschriht, Zeitschrift Electrochem. 30, 508-516.

Verwey, E. J. W., and Overbeek, J. Th. G., 1948. Theory of the Stability of Lyophobic Colloids, *Elsevier*. Amsterdam, 51(3), 631-636.

Yamada, S., Sakai, T., Nakano, M., Noda, T., 2022. Method to introduce the cementation effect into existing elasto-plastic constitutive models for soils, *J. Geotech. Geoenviron. Eng*. 148, 04022013.